



This is a repository copy of *Competitive metal-coordination of hexaaminotriphenylene on Cu(111) by intrinsic copper versus extrinsic nickel adatoms.*

White Rose Research Online URL for this paper:
<https://eprints.whiterose.ac.uk/139553/>

Version: Supplemental Material

Article:

Lischka, M., Dong, R., Wang, M. et al. (6 more authors) (2019) Competitive metal-coordination of hexaaminotriphenylene on Cu(111) by intrinsic copper versus extrinsic nickel adatoms. *Chemistry - A European Journal*, 25 (8). pp. 1975-1983. ISSN 0947-6539

<https://doi.org/10.1002/chem.201803908>

This is the peer reviewed version of the following article: Lischka, M. , Dong, R. , Wang, M. , Martsinovich, N. , Fritton, M. , Grossmann, L. , Heckl, W. ., Feng, X. and Lackinger, M. (2018), Competitive metal-coordination of hexaaminotriphenylene on Cu(111) by intrinsic copper versus extrinsic nickel adatoms. *Chem. Eur. J.*, which has been published in final form at <https://doi.org/10.1002/chem.201803908>. This article may be used for non-commercial purposes in accordance with Wiley Terms and Conditions for Self-Archiving.

Reuse

Items deposited in White Rose Research Online are protected by copyright, with all rights reserved unless indicated otherwise. They may be downloaded and/or printed for private study, or other acts as permitted by national copyright laws. The publisher or other rights holders may allow further reproduction and re-use of the full text version. This is indicated by the licence information on the White Rose Research Online record for the item.

Takedown

If you consider content in White Rose Research Online to be in breach of UK law, please notify us by emailing eprints@whiterose.ac.uk including the URL of the record and the reason for the withdrawal request.



eprints@whiterose.ac.uk
<https://eprints.whiterose.ac.uk/>

1. Additional STM data

-high temperature annealing:

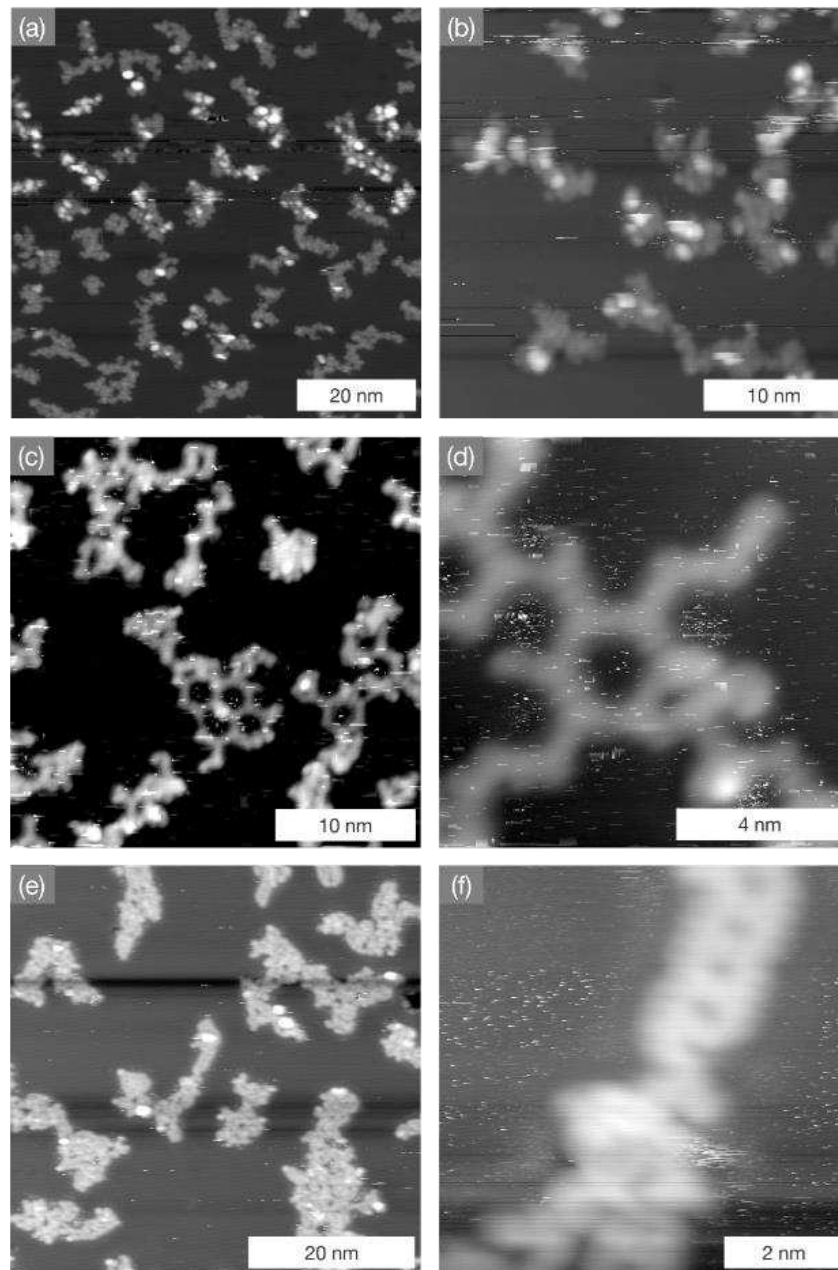


Figure S1. a) overview and b) close-up STM images of HATP on pristine Cu(111) acquired after annealing to 300 °C. The network sizes are relatively small and internal details of these less

regular structures were not resolved, presumably due to decomposition of the molecules. c) overview and d) close-up STM images of HATP on nickel-covered Cu(111) acquired after annealing to 260 °C, showing still intact organometallic networks; e) overview and f) close-up STM images of HATP on nickel-covered Cu(111) acquired after annealing to 300 °C. Similar to pristine Cu(111) the structures are mostly irregular due to decomposition of the molecules. (tunneling parameters: a) 1.72 V, 77 pA; b) 3.83 V, 88 pA; c) 2.61 V, 59 pA; d) 1.28 V, 95 pA; e) 3.83 V, 88 pA; f) 1.24 V, 34 pA)

-annealing to 200 °C with reduced heating and cooling rates:

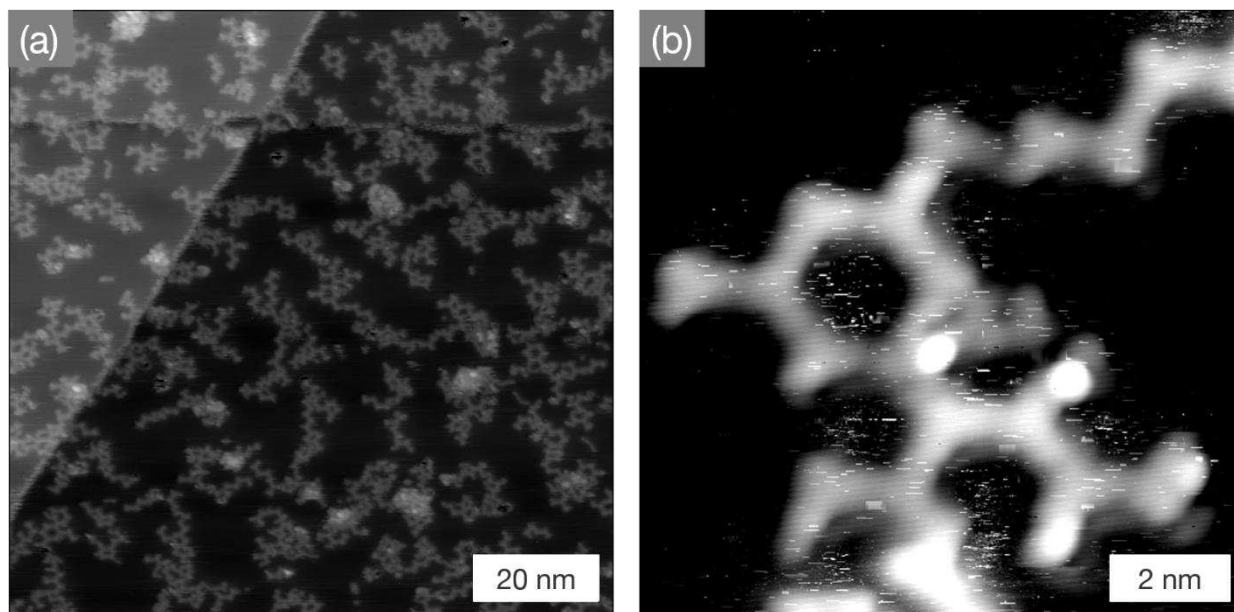


Figure S2. a) overview and b) close-up STM images of HATP on nickel-covered Cu(111) acquired after annealing to 200 °C with a reduced heating and cooling rate of 0.86 °C min⁻¹. No obvious improvement of the structural quality was observed in comparison to experiments with the normally applied heating and cooling rate of 1.66 °C min⁻¹. (tunneling parameters: a) 2.61 V, 59 pA; b) 1.28 V, 95 pA)

-hexamer stability:

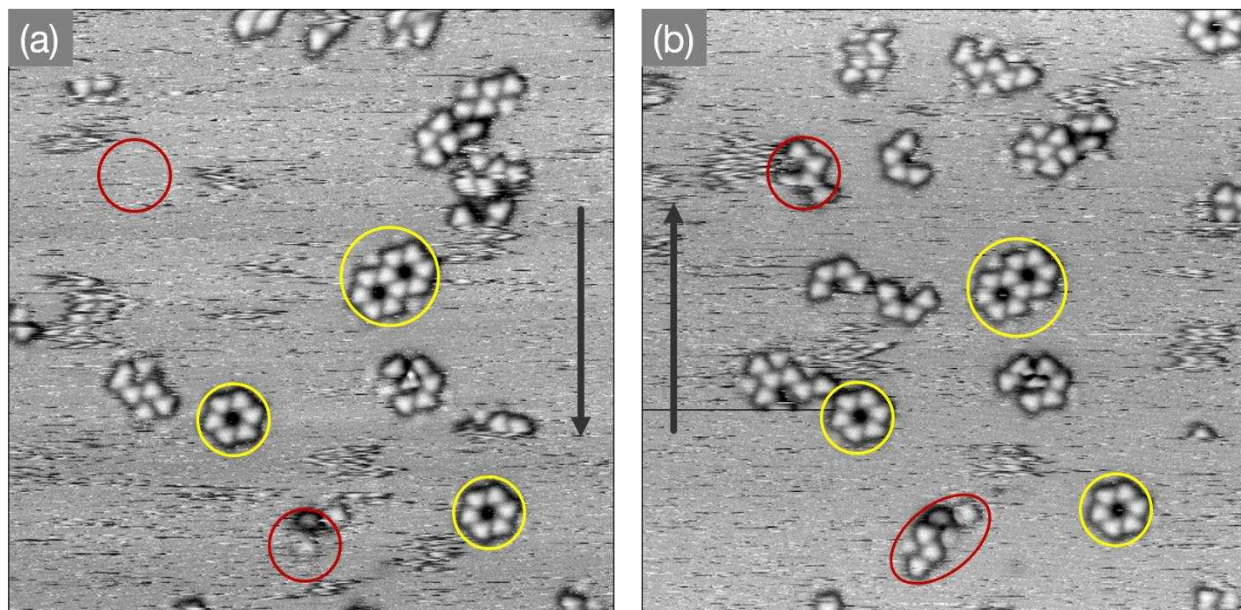


Figure S3. STM image acquired after room temperature deposition of HATP onto pristine Cu(111). a) and b) show two subsequently acquired images, the vertical arrows indicate the slow scan direction; while less compact aggregates (examples marked in red) undergo considerable changes, the cyclic hexamers (marked in yellow) remain unchanged; this indicates overall weak intermolecular interactions as well as a relatively high stability of the hexamers and analogous structures; (image size $30 \times 30 \text{ nm}^2$; tunneling parameters: 0.73 V, 53 pA;)

-overview images:

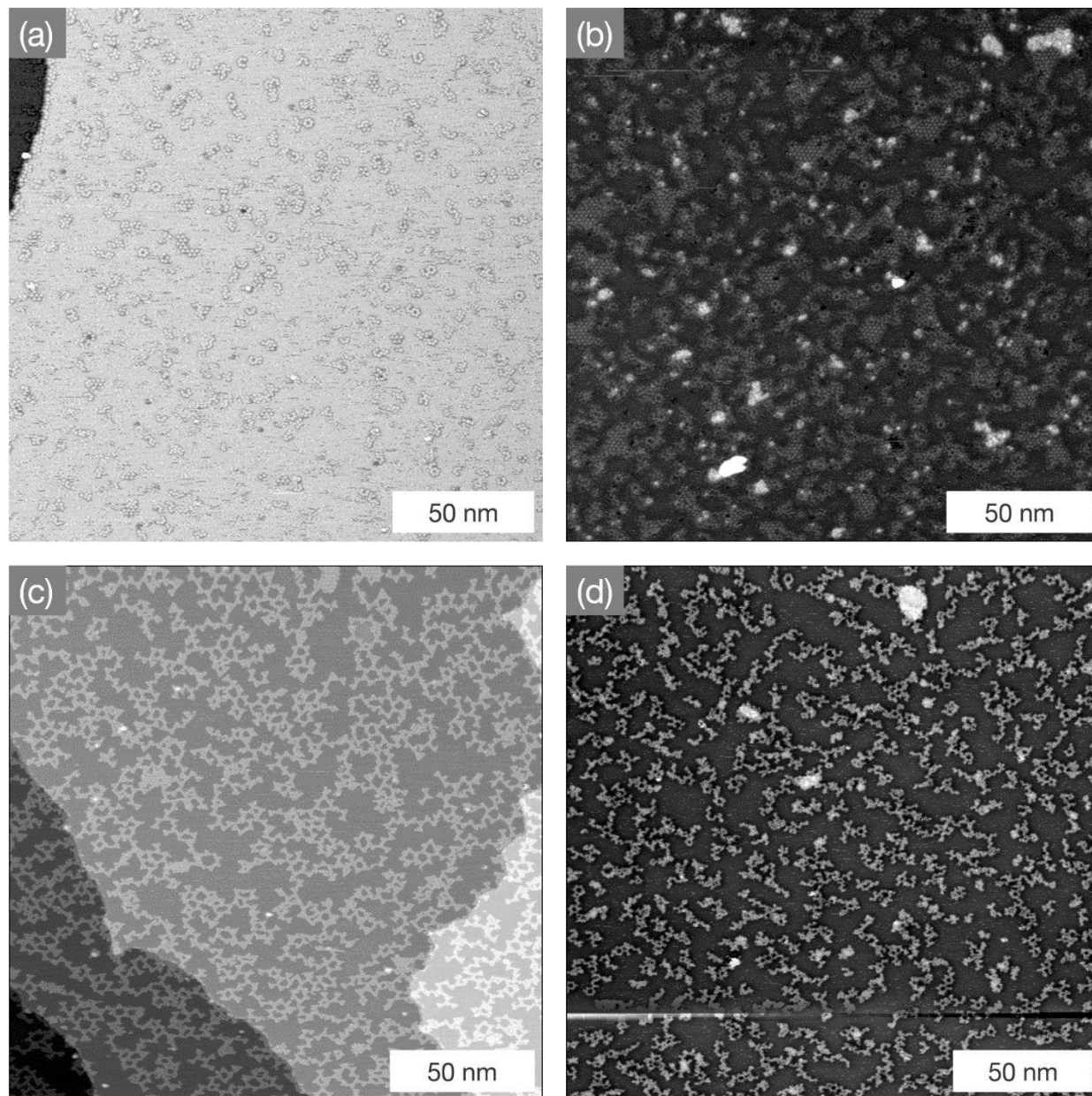


Figure S4. Overview STM images acquired after room temperature deposition of HATP (upper row) and subsequent annealing to 200 °C (lower row) on a) / c) pristine Cu(111), and b) / d) nickel-covered Cu(111); (tunneling parameters: a) 0.80 V, 61 pA; b) 0.87 V, 92 pA; c) 0.92 V, 91 pA; d) 0.91 V, 95 pA)

2. Additional XPS data

-high temperature annealing:

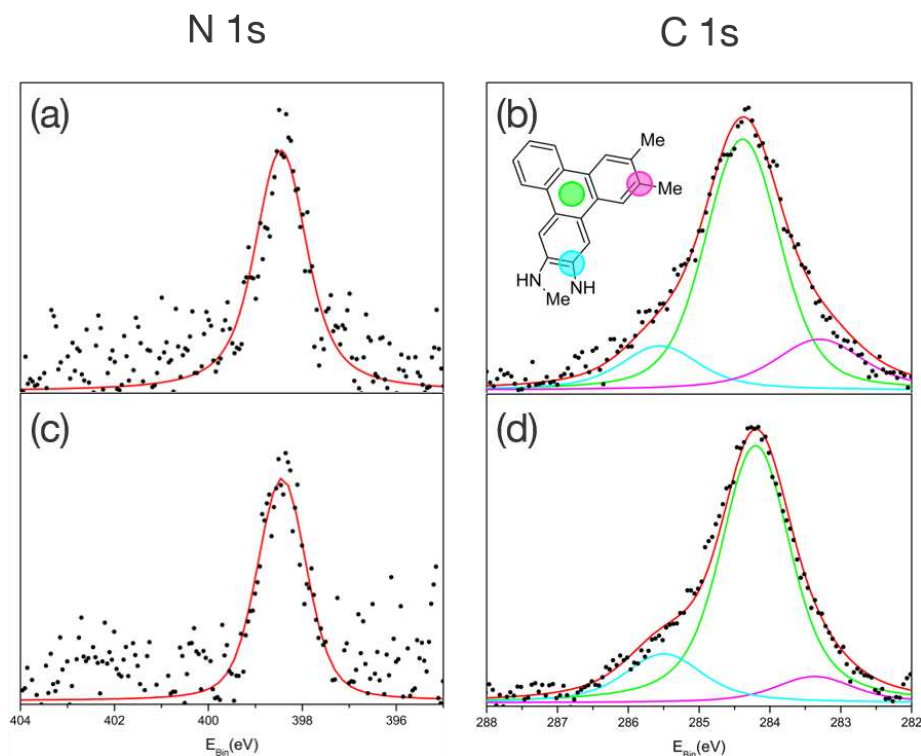


Figure S5. N 1s (left) and C 1s (right) XP spectra of HATP acquired on a) / b) pristine Cu(111), and c) / d) nickel-covered Cu(111) after annealing to 300 °C for 10 min. On both surfaces, the high temperature annealing results in intensity losses of both N 1s (pristine Cu(111) ~ 43% / Cu(111) + Ni: ~72%) and C 1s (pristine Cu(111) ~ 84% / Cu(111) + Ni: ~78%). The values in parentheses indicate the ratio of the remaining intensities to the intensities measured directly after room temperature deposition. On pristine Cu(111), the relative loss of nitrogen is considerably higher than that of carbon, indicating decomposition of the molecules by dissociation of amino groups. This is in line with the emergence of an additional low BE shoulder in C 1s at ~283.2 eV. This shoulder can be interpreted as an organometallic carbon-metal bond (C-M),^[1] in line with the similarly observed integral shift of the C 1s peak by +0.15

eV to lower BE as compared to the value after annealing to 200 °C.^[2] Formation of organometallic bonds indicates dissociation of carbon-nitrogen bonds.

-additional experiments with larger amounts of co-deposited Ni

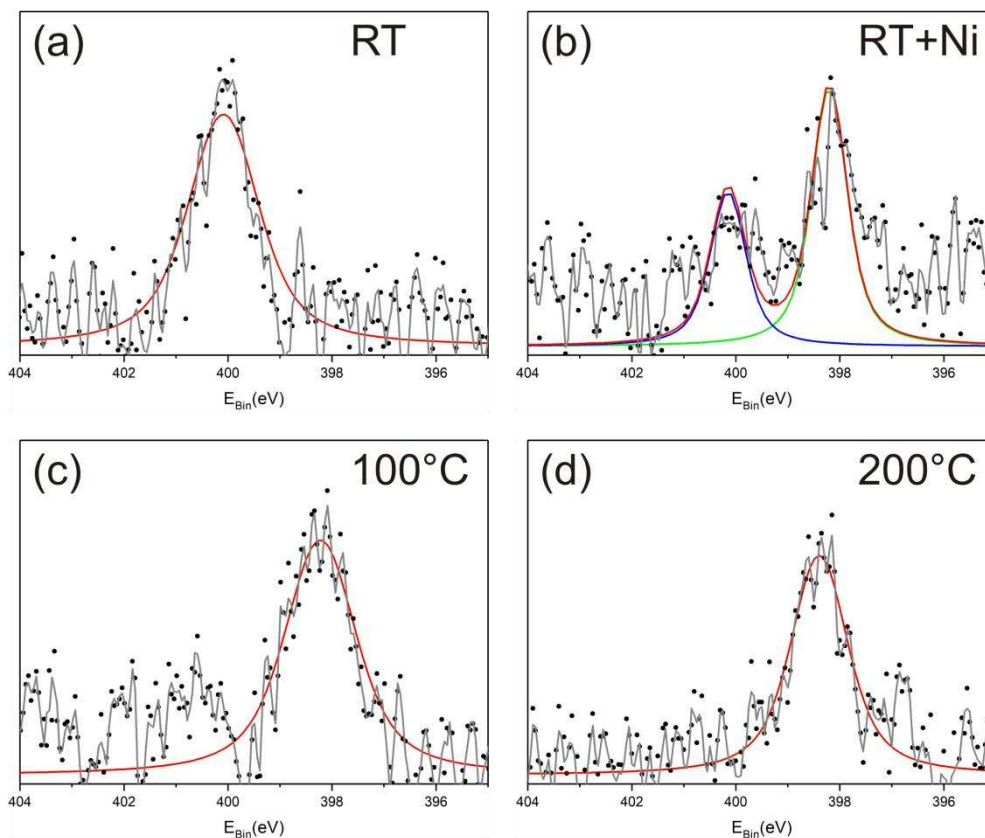


Figure S6. N 1s spectra acquired on Cu(111) after a) room temperature deposition of HATP; b) co-deposition of Ni; c) subsequent annealing to 100 °C; d) subsequent annealing to 200 °C; The amount of co-deposited Ni was approximately 5 times higher as compared to the experiments shown in Figure 5 of the main manuscript, whereas the amount of HATP was kept constant. Black dots represent raw data after background subtraction, the grey lines correspond to smoothed data (Savitzky-Golay, 5 point); the blue, green, and red curves represent fits. In accord with the data shown in Figure 5, co-deposition of Ni induced an initial deprotonation already at room temperature. However, full deprotonation still required further sample annealing. Yet, the degree of deprotonation after annealing to 100 °C is higher for the larger amount of Ni.

3. Additional DFT simulations

All structure files can be downloaded from: <https://figshare.com/s/e5573906428dfbf16dfa>

-possible structural models for the self-assembled hexamers:

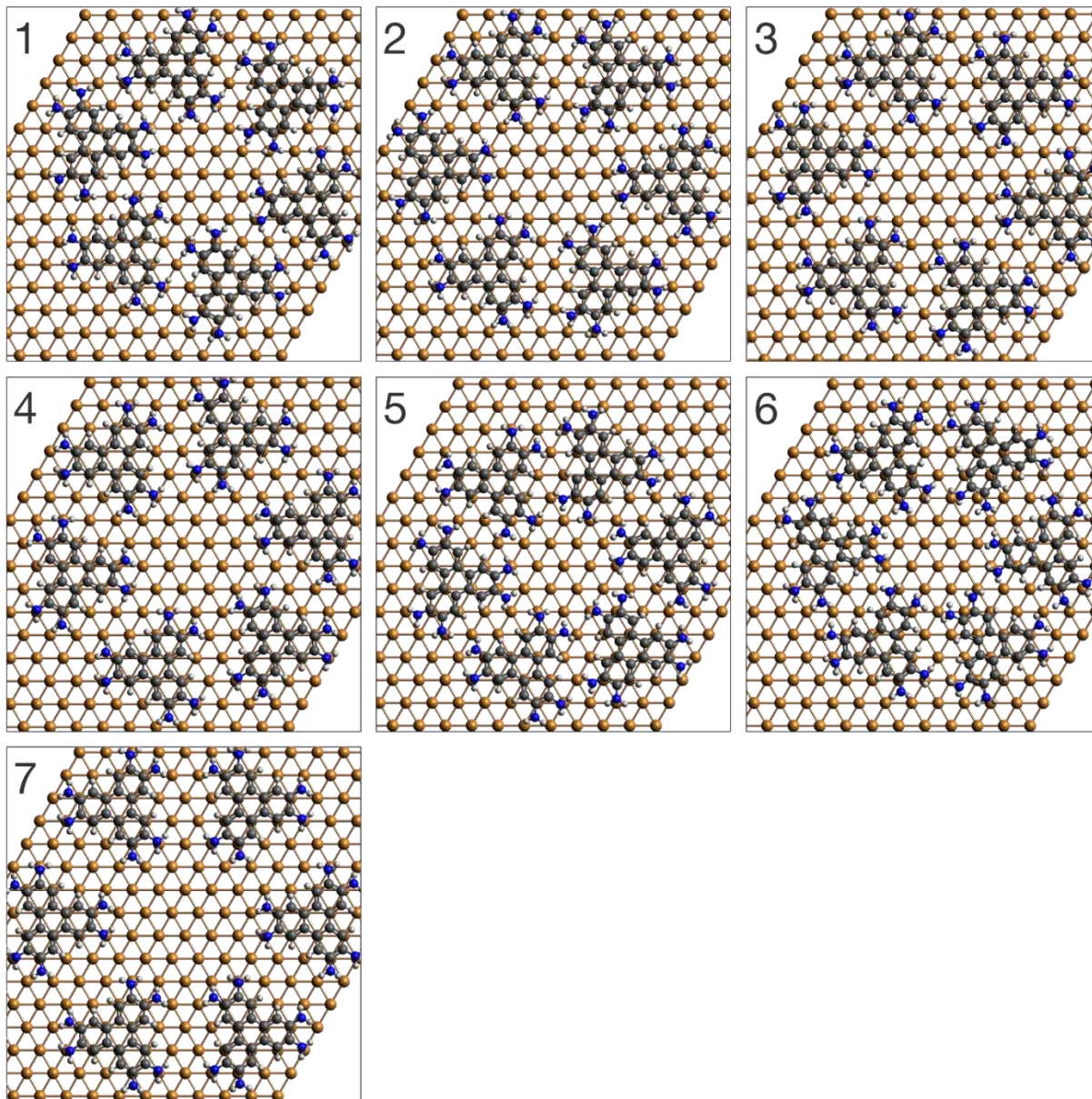


Figure S7. DFT-optimized geometries for the self-assembled cyclic hexamers of non-deprotonated HATP molecules on pristine Cu(111). The simulations were carried out on a two-layer copper slab, but only one slab is shown for clarity. Seven competing models with comparable intermolecular distances are presented that are all consistent with the experimental

result within the experimental error. Moreover, the binding energies of all models are rather similar. These simulations reveal a pronounced adsorption-site preference of HATP molecules, where all aromatic rings of the triphenylene backbone reside above three-fold hollow sites of the Cu(111) surface; all binding energies and structural parameters are summarized in Table S1.

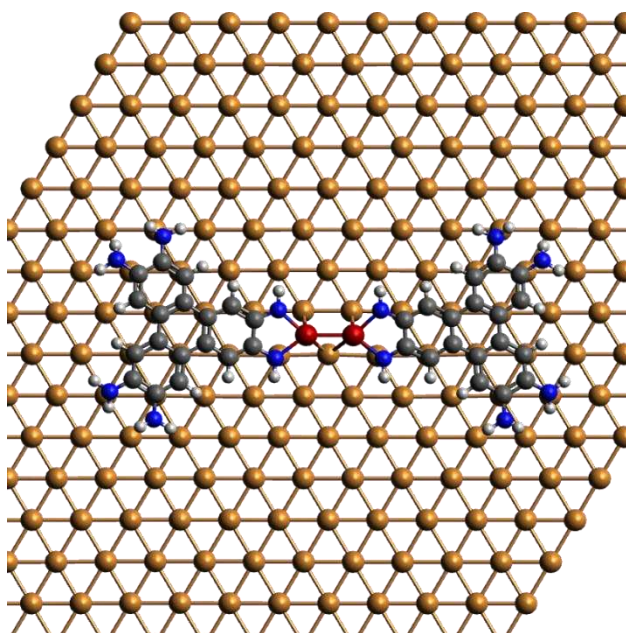


Figure S8. DFT-optimized geometry of a metal-organic HATP dimer on Cu(111) with an axially aligned Cu_2 coordination center. The center-to-center distance between the two molecules of 1.55 nm in this model is in perfect agreement with the experimental value of (1.55 ± 0.08) nm. The average adsorption height (excluding hydrogen atoms) of HATP above Cu(111) structure amounts to (2.77 ± 0.27) Å, i.e. comparable to the other metal-coordinated structures.

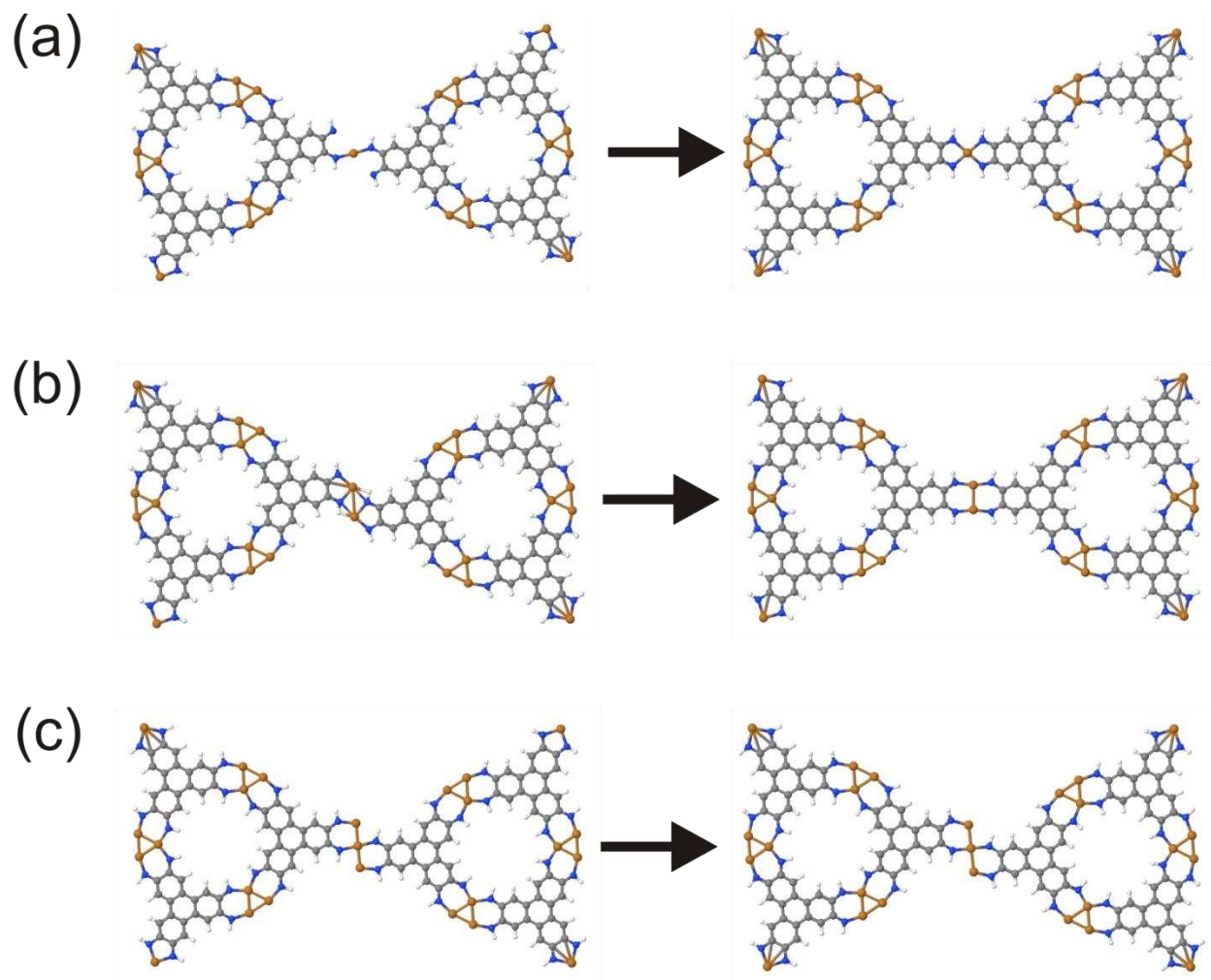


Figure S9. DFT simulations of conceivable metal-coordination bonds interlinking two Cu_3 -coordinated supramolecular trimers based on a) one, b) two, and c) three coordinating Cu atoms. Starting geometries are shown on the left hand side, the corresponding optimized geometries are depicted on the right hand side. While the configurations shown in a) and b) result in straight links, only the configuration shown in c) can reproduce the experimentally observed kink along the bond axis.

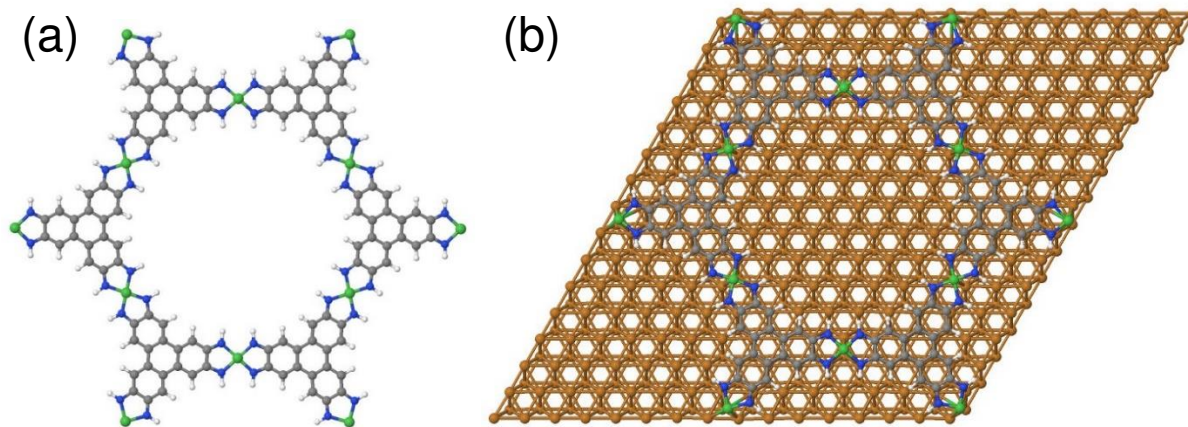


Figure S10. DFT-optimized geometries of Ni-coordinated HATP hexamers a) in the gas phase and b) adsorbed on Cu(111). The gas phase calculations result in a center-to-center distance between adjacent HATP molecules of 1.27 nm, perfectly corresponding to 5 times the Cu(111) lattice parameter (1.28 nm). Note that DFT optimization of the Cu(111) lattice parameter results in a value of 0.259 nm, i.e. about 2% larger than the experimental value of 0.255 nm. Nevertheless, DFT simulations of the Ni-coordinated honeycomb network as a commensurate $5\sqrt{3} \times 5\sqrt{3}R30^\circ$ superstructure (i.e. the molecular lattice is rotated by 30° with respect to the Cu(111) lattice), indicate a perfect match. The two non-equivalent HATP molecules within one unit-cell can simultaneously adopt their preferred adsorption sites with the centers of all aromatic rings above fcc-sites. Interestingly, the corresponding HATP adsorption height (without hydrogen atoms) of $(2.48 \pm 0.12) \text{ \AA}$ is notably lower than that of the Cu-coordinated structures.

Table S1. Binding energies and structural parameters for the models of the cyclic hexamers shown in Fig. S7. E_{total} denotes the total binding energy including contributions from molecule-surface and molecule-molecule interactions ($E_{\text{total}} = [E_{\text{hexamer on Cu}} - E_{\text{Cu}} - 6 E_{\text{HATP}}] / 6$), whereas $E_{\text{molecule-molecule}}$ refers to the intermolecular binding energies ($E_{\text{molecule-molecule}} = [E_{\text{hexamer in vacuum}} - 6 E_{\text{HATP}}] / 6$), evaluated for the unchanged structures of the adsorbed species. For the models 3, 4, 6, and 7 all aromatic rings of each of the six molecules reside above similar three-fold hollow sites (either fcc or hcp). In these cases, the binding energies were also evaluated for the respective other three-fold hollow site. $d_{\text{mol-mol}}$ refers to the center-to-center distance of two diametrically opposed HATP molecules. These distances were measured between the centers of mass of the HATP molecules, whereby the values for all three possible pairs of diametrically opposed HATP molecules were found to be similar within the reported accuracy.


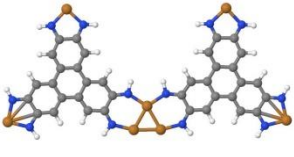


model #	E_{total} (eV/molecule)	$E_{\text{molecule-molecule}}$ (eV / molecule)	$d_{\text{mol-mol}}$ (nm)
1	-4.04	-0.12	2.235
2	-4.08	-0.17	2.352
3-fcc	-4.11	-0.16	2.378
3-hcp	-4.07	-0.16	2.378
4-fcc	-4.11	-0.17	2.399
4-hcp	-4.07	-0.16	2.399
5	-4.00	-0.08	2.165
6-fcc	-3.99	-0.06	2.140
6-hcp	-3.98	-0.07	2.140
7-fcc	-4.13	-0.18	2.591
7-hcp	-4.11	-0.17	2.591

Table S2. Binding energies of metal-coordinated molecular dimers, defined as

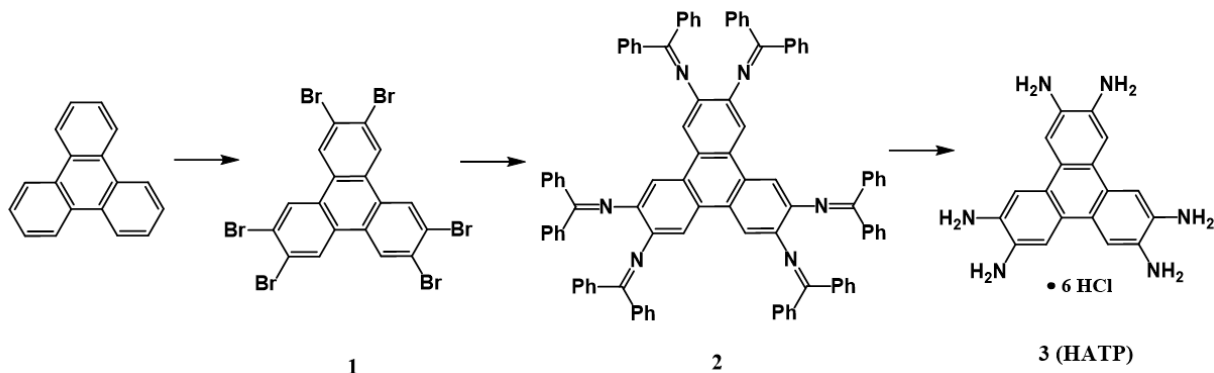
$$E_{\text{binding}} = [E_{\text{metal-coordinated dimer}} - n E_{\text{M}} - 2 E_{\text{HATP}}],$$

where n is the number of coordinating metal atoms, E_{M} is the energy of one metal atom, and

E_{HATP} corresponds to the energy of a singly deprotonated HATP molecule.

Coordinating metal atom or cluster	Structure	E_{binding} (eV)
Cu ₁		-5.97
Cu ₃ triangle		-9.82
Cu ₃ kinked		-8.52
Ni ₁		-9.68

4. HATP synthesis



The synthesis of compound **2** and **3** were carried out according to the previous reported literature.^[3]

2,3,6,7,10,11-hexabromotriphenylene (1): To a mixture of triphenylene (2 g, 8.8 mmol) and iron (0.21 g, 3.7 mmol) in 100 mL nitrobenzene was added bromine (4.56 ml, 177.7 mmol) dropwise under argon. The mixture was stirred at room temperature for 30 min and heated at 210 °C for 3 h. After cooling to room temperature, 300 mL diethyl ether was added. The crude product was filtered, washed with acetone and chloroform, and recrystallized in 1,2-dichlorobenzene to give **1** (5.5 g, 7.8 mmol) as white solid with 89 % yield. The product was used directly for the next step.

2: To a mixture of **1** (2 g, 2.85 mmol), tris(dibenzylideneacetone)dipalladium(0) (0.63 g, 0.69 mmol), rac-BINAP (0.86 g, 1.38 mmol) and sodium tert-butoxide (2.14 g, 22.23 mmol) in toluene (70 mL), benzophenone imine (3.73 mL, 22.23 mmol) was added under argon. The mixture was degassed by three freeze-pump-thaw cycles, purged with argon, and stirred at 125 °C for 24 h. After cooling to room temperature, it was filtered through Celite, washed with DCM, and then evaporated. The crude product was purified by column chromatography on silica

gel with AcOEt/hexane (1:3) as eluent, to give **2** (3 g, 2.3 mmol) as yellow solid in 81% yield. ^1H NMR (CD_2Cl_2) δ (ppm) 7.73 – 7.66 (m, ^1H), 7.48 – 7.31 (m, ^4H), 7.29 – 7.16 (m, ^4H), 7.10 (s, ^1H), 7.02 – 6.96 (m, 1H). HR MALDI-TOF MS for $\text{C}_9\text{H}_{66}\text{N}_6$ (calcd. 1302.5349): $m/z = 1302.5979$.

HATP (**3**): To a solution of **2** (660 mg, 0.51 mmol) in THF (30 mL), a 2.0 M aqueous HCl solution (1.5 mL, 3 mmol) was added. The mixture was stirred at room temperature for 30 min. The precipitate was filtered, washed with N_2 bubbled acetone and DCM, and dried under vacuum, to give **3** (236 mg, 0.44 mmol) as off-white solid in 87% yield. ^1H NMR (DMSO) δ (ppm) 7.83 (s, ^1H), 3.79 (s, ^2H). HR MALDI-TOF MS for $\text{C}_{18}\text{H}_{18}\text{N}_6$ (calcd. 318.1593): $m/z = 318.1599$.

5. References

- [1] a) R. Gutzler, L. Cardenas, J. Lipton-Duffin, M. E. Garah, L. E. Dinca, C. E. Szakacs, C. Fu, M. Gallagher, M. Vondráček, M. Rybachuk, D. F. Perepichka, F. Rosei, *Nanoscale* **2014**, *6*, 2660-2668; b) J. Bushell, A. F. Carley, M. Coughlin, P. R. Davies, D. Edwards, D. J. Morgan, M. Parsons, *J. Phys. Chem. B* **2005**, *109*, 9556-9566.
- [2] a) T. A. Pham, F. Song, M.-T. Nguyen, Z. Li, F. Studener, M. Stöhr, *Chem. Eur. J.* **2016**, *22*, 5937-5944; b) M. Lischka, M. Fritton, J. Eichhorn, V. S. Vyas, T. Strunskus, B. V. Lotsch, J. Björk, W. M. Heckl, M. Lackinger, *J. Phys. Chem. C* **2018**, *122*, 5967-5977.
- [3] L. Chen, J. Kim, T. Ishizuka, Y. Honsho, A. Saeki, S. Seki, H. Ihee, D. Jiang, *J. Am. Chem. Soc.* **2009**, *131*, 7287-7292.